Title

New constraints on the variation of the geomagnetic field during the late Neolithic period: Archaeointensity results from Sichuan, southwestern China

Authors

Cai, S
Chen, W
Tauxe, L
et al.

Publication Date

2015

DOI

10.1002/2014JB011618

Peer reviewed

AGU PUBLICATIONS

JGR

Journal of Geophysical Research: Solid Earth

RESEARCH ARTICLE
10.1002/2014JB011618

Key Points:
- High-fidelity archaeointensity results around 3000 B.C.E. in southwestern China
- A broad trough of the geomagnetic intensity between ~3000 and 2000 B.C.E.
- Reliable inputs to improve the eastern Asian model and global models

Supporting Information:
- Readme
- Table S1

Correspondence to:
S. Cai,
shuhui.cai08@gmail.com

Citation:
Cai, S., W. Chen, L. Tauxe, C. Deng, H. Qin, Y. Pan, L. Yi, and R. Zhu (2015), New constraints on the variation of the geomagnetic field during the late Neolithic period: Archaeointensity results from Sichuan, southwestern China, *J. Geophys. Res. Solid Earth*, *120*, 2056–2069, doi:10.1002/2014JB011618.

Received 18 SEP 2014
Accepted 22 FEB 2015
Accepted article online 25 FEB 2015
Published online 8 APR 2015

New constraints on the variation of the geomagnetic field during the late Neolithic period: Archaeointensity results from Sichuan, southwestern China

Shuhui Cai[1], Wei Chen[2], Lisa Tauxe[3], Chenglong Deng[1], Huafeng Qin[4], Yongxin Pan[4], Liang Yi[1], and Rixiang Zhu[1]

[1]State Key Laboratory of Lithospheric Evolution, Institute of Geology and Geophysics, Chinese Academy of Sciences, Beijing, China, [2]The Sichuan Provincial Cultural Relics and Archeology Research Institute, Chengdu, China, [3]Scripps Institution of Oceanography, University of California, San Diego, California, USA, [4]Key Laboratory of the Earth and Planetary Physics, Institute of Geology and Geophysics, Chinese Academy of Sciences, Beijing, China

Abstract We have carried out an archaeomagnetic study on a late Neolithic locality (Liujiazhai) in Sichuan, southwestern China. We pull together various dating techniques, including radiocarbon analysis, optically stimulated luminescence dating, stratigraphic information as well as archaeological and archaeomagnetic estimations, to constrain the age of the studied samples. Rock magnetic results indicate thermally stable fine-grained magnetite or titanomagnetite as the dominant magnetic carriers. More than half of the specimens (141/246) in the paleointensity experiment pass the selection criteria and are considered to record robust intensity values. The virtual axial dipole moments range from approximately (2.8 to 7.8) $\times 10^{22}$ Am^2 with an average of 5.9×10^{22} Am^2, indicating that the geomagnetic intensity around 3000 before the Common Era (B.C.E.) is overall lower than the present field intensity (9.8×10^{22} Am^2) of this area. The new results from Liujiazhai are generally consistent with the published data of similar age but deviate from the only available model of CALS10k.1b at certain time periods, making them important for future improvements of the model. Those data are significant for constraining the variation of geomagnetic field intensity between ~3100 and 2600 B.C.E. and improving the regional model of eastern Asia.

1. Introduction

The geomagnetic field is one of the most important basic physical properties of the Earth, with a history of at least ~3.5 Ga [*Tarduno et al.*, 2010; *Biggin et al.*, 2011; *Usui et al.*, 2009]. The field is generated by convections in the Earth's fluid outer core, and thus, it is a window to the Earth's deep interior. The variation of the geomagnetic field may have significant dynamical implications. For instance, core-mantle interactions and heat flow may influence geomagnetic variations [*Bloxham*, 2000; *Willis et al.*, 2007; *Biggin et al.*, 2012; *Hori et al.*, 2014]. Velocity changes in outer-core flow might cause geomagnetic jerks [*Bloxham et al.*, 2002; *Dumberry and Finlay*, 2007; *Olsen and Mandea*, 2008; *Mandea et al.*, 2010]. The geomagnetic field played a key role in the evolution of life on the Earth as well, almost certainly early on, by shielding against cosmic radiation, but also recently aiding processes such as animal navigation [*Tarduno et al.*, 2010; *Pan and Zhu*, 2011; *Wiltschko and Wiltschko*, 2012]. Potential connections between the geomagnetic field and global climate have been discussed in many studies [*Kent*, 1982; *Gallet et al.*, 2005, 2014; *Courtillot et al.*, 2007; *Bard and Delaygue*, 2008]. Therefore, investigating the evolution of the geomagnetic field is crucial for a better understanding of the environment and state of the Earth.

The direction and intensity of the ancient geomagnetic field can be obtained from direct observations (with a history of ~400 years for direction and <200 years for intensity); archaeomagnetic artifacts such as pottery, brick, and baked clay (~10 kyr); and paleomagnetic records from volcanics and sediments (~3.5 Ga). The direct observational data are far too limited to represent the whole evolution history of the geomagnetic field. Thus, archaeomagnetic and paleomagnetic studies are quite necessary. Archaeomagnetic studies focus on the detailed evolution of the geomagnetic field over the past few thousand years and have a potential application for archaeomagnetic dating [*Ben-Yosef et al.*, 2008, 2010; *Pavón-Carrasco et al.*, 2009, 2011; *Aguilar Reyes et al.*, 2013]. China is located over one of the largest magnetic anomalies

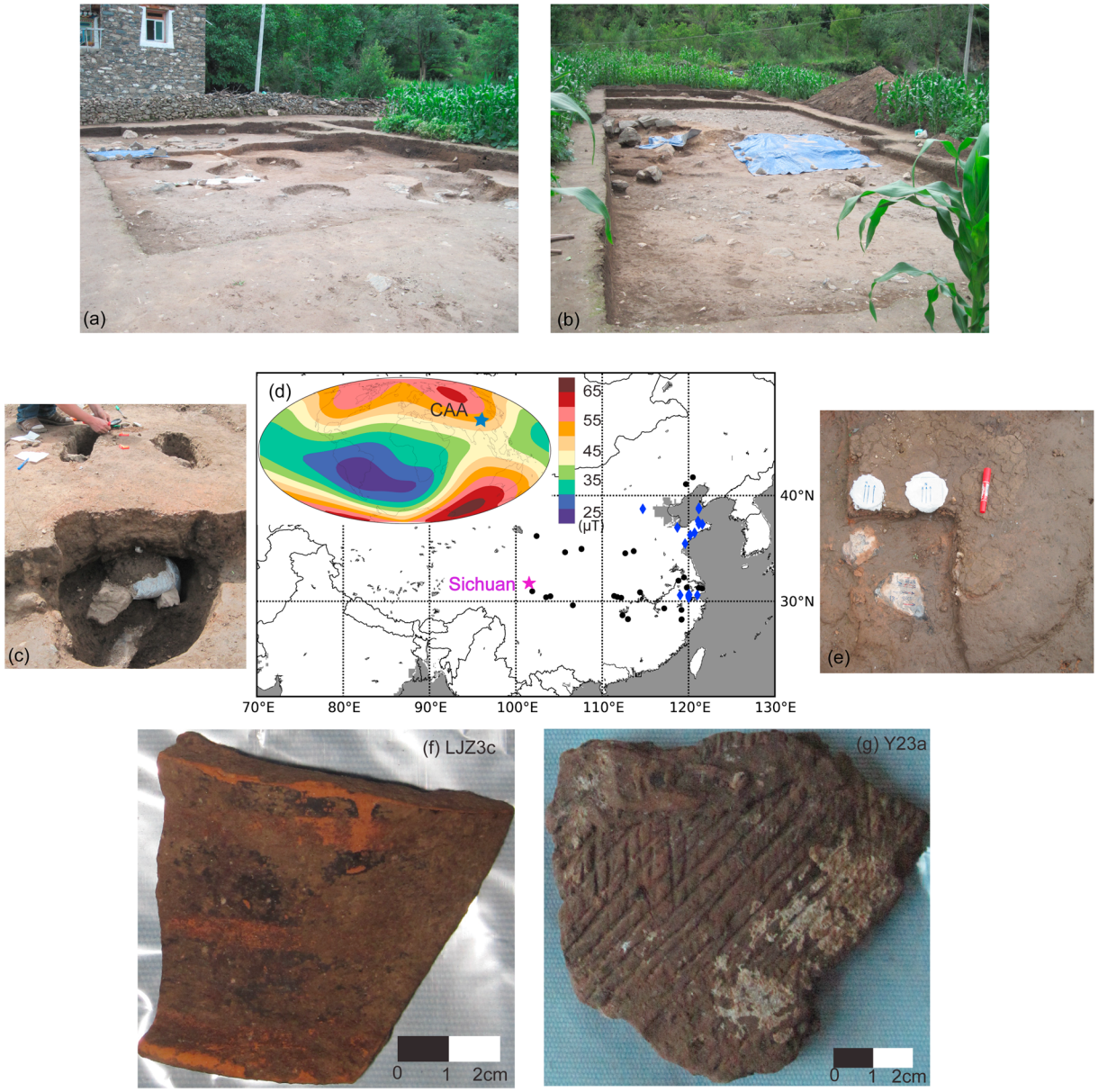

Figure 1. (a and b) Photographs of sampling site. (c and e) Oriented samples collected from the kilns. (d) Sitemap of Liujiazhai site and published data in China. The black solid circles represent the locations of the accepted archaeointensity data in China from MagIC database. For data selection criteria, please see the text. The magenta star is the location of this study. The blue diamonds represent the published data locations in *Cai et al.* [2014]. The inset is the intensity of the geomagnetic field in the 2015 International Geomagnetic Reference Field over the surface of the Earth with the central Asian anomaly (CAA). The blue star in the inset shows the location of sampling site in this study. (f and g) Representative pottery fragments in this study.

on Earth (the central Asian anomaly labeled CAA in the inset of Figure 1d). The growth, decay, and motion of the CAA and other so-called "flux patches" are the subject of intense research [*Amit et al.*, 2011; *Korte et al.*, 2011]. Understanding the variations of the geomagnetic field in China is important for understanding the evolution of these anomalies. However, the published data in China, even in all of eastern Asia, are sparse and scattered [*Cai et al.*, 2014; *Yu*, 2012]. Most of the existing Chinese data are focused in the eastern part of China and are mainly from the past 3 kyr. In this study, we present new paleointensity results from Liujiazhai site in Sichuan province, southwestern China, a cultural locality dated to ~3000 before the Common Era (B.C.E.), which will fill many gaps of the present data set in both time and space.

Table 1. Sample Information Analyzed in This Study[a]

Site/Sample	Age	Dating Method	Material	N/n
LJZ1a	3100 ± 250 B.C.E.	AE	Pottery	1/9
LJZ1c	2895 ± 253 B.C.E.	OSL	Pottery	1/6
LJZ1d	3004 ± 87 B.C.E.	AE + Stra	Pottery	1/7
LJZ2b	2893 ± 27 B.C.E.	AE + Stra	Pottery	1/8
LJZ2c	3004 ± 87 B.C.E.	AE + Stra	Pottery	1/7
LJZ2d	3004 ± 87 B.C.E.	AE + Stra	Pottery	1/6
LJZ3c	3011 ± 95 B.C.E.	AE + Stra	Pottery	1/9
LJZ3d	2725 ± 98 B.C.E.	AE + Stra	Pottery	1/6
LJZ3e	3011 ± 95 B.C.E.	AE + Stra	Pottery	1/7
LJZ4a	2622 ± 260 B.C.E.	OSL	Pottery	1/9
LJZ4e	2622 ± 260 B.C.E.	AE + Stra	Pottery	1/7
LJZ4f	2725 ± 98 B.C.E.	AE + Stra	Pottery	1/7
Y2	4870–4816 B.P.	AE + Stra	Burnt clay	4/27
Y3	4726–4528 B.P.	^{14}C	Burnt clay	3/16
Y4	5055–4866 B.P.	^{14}C	Burnt clay	7/35
Y5	5041–4867 B.P.	^{14}C	Burnt clay	6/32
Y6	3011 ± 95 B.C.E.	AE + Stra	Burnt clay	3/15
Y7	3011 ± 95 B.C.E.	AE + Stra	Burnt clay	2/11
Y8	4773–4577 B.P.	^{14}C	Burnt clay	4/22

[a]Dating method "AE" means archaeological estimation. OSL is the optically stimulated luminescence method. Stra means stratigraphic information. ^{14}C is the radiocarbon dating method. N/n is the number of samples/specimens.

2. Sampling

The Liujiazhai site is located at the upriver of Dadu River in Sichuan province, southwestern China (31° 47′57″N, 101°32′02″E) (Figure 1d). The characteristics of excavated materials (such as shape and decoration of potteries, style of kilns, and contents of tombs) indicate that the Liujiazhai site belongs to the late Neolithic period with a main age of ~3000 B.C.E. Painted pottery is one of the representative characteristics in this area over that period. In order to rescue the precious relics from an impending construction project, this site was excavated twice in 2011 and 2012. In total, five cultural layers were uncovered with various artifacts such as pottery kilns, ash pits, and house vestiges. The accumulation thickness of each layer varies from 20 to 180 cm. The styles of the unearthed house vestiges evolved with different cultural layers, showing that there might be continuous human beings activity here. A huge number of pottery fragments, burnt clay, and animal bones were unearthed, which indicate that the pottery industry was active that time. The samples studied in this paper were collected from the areas excavated in 2012 (Figures 1a and 1b) and were mainly assigned to the first three cultural layers. Both oriented in situ (Figures 1c and 1e) and unoriented (Figures 1f and 1g) samples were collected for directional and paleointensity studies. Here we discuss the intensity results. The directional results will be described elsewhere.

With respect to sample nomenclature, the pottery fragments are labeled LJZ. In specimen LJZ1a-01, for instance, "1a" is the sample name and "01" is the specimen name. The samples of burnt clay collected from kilns are named after the kiln name Yx. The "x" is the number of the kiln, Y1, Y2, Y3, and so on. For example, in Y22a-01, "Y2" is the kiln name, "2a" is the sample name, and 01 is the specimen name.

For the purpose of obtaining more precise ages for the samples, materials suitable for radiocarbon dating were collected where available. For instance, plant ashes from kilns Y1 and Y8, charcoals from Y3 and Y4, and a piece of animal bone from Y5 were collected. Besides, two pottery samples of LJZ1c and LJZ4a were selected for optically stimulated luminescence (OSL) dating. The sampling information is listed in Table 1.

3. Methods

3.1. Dating Techniques

The materials collected for radiocarbon dating were analyzed by Beta Analytic Inc, Florida, USA, where the accelerator mass spectrometry dating method was adopted. Charred materials from Y1, Y3, Y4, and Y8 and bone collagen from Y5 were extracted for radiocarbon analysis.

Sample preparation and analysis for OSL dating was conducted in the OSL laboratory, Institute of Geology and Geophysics, Chinese Academy of Sciences. Totals of 13 and 10 aliquots were measured for equivalent dose determination for LJZ1c and LJZ4a, respectively. The concentrations of uranium (U), thorium (Th), and potassium (K) involved in dose rate calculations were measured in the China Institute of Atomic Energy in Beijing. The cosmic ray dose rate was estimated according to *Prescott and Hutton* [1994], and the dose rate of each sample was calculated following the method of *Aitken* [1998].

3.2. Rock Magnetism

In order to determine the rock magnetic properties such as mineralogy and domain state of the samples, different rock magnetic experiments were employed. Hysteresis loops, acquisition curves of isothermal remanent magnetization (IRM), and first-order reversal curves (FORCs) [*Roberts et al.*, 2000] were measured with the MicroMag 3900 Vibrating Sample Magnetometer in the Paleomagnetism and Geochronology Laboratory (PGL) at the Institute of Geology and Geophysics, Chinese Academy of Sciences, Beijing. The variability of magnetization versus temperature (*M-T*) was measured with the magnetic measurements variable field translation balance fixed with an oven in the PGL, which helps detect the Curie temperature (T_c) and thermostability of the minerals. Three-axis IRM demagnetization experiments [*Lowrie*, 1990] were conducted to further constrain the mineralogy and coercivity distribution of the samples. During these experiments, fields of 2.5 T, 0.5 T, and 0.15 T were applied along the *x*, *y*, and *z* axes successively. The resulting IRM was thermally demagnetized in a stepwise fashion with a magnetic measurement thermal demagnetizer super cooled (MMTDSC) oven designed by John Shaw and measured with the 2G 760 superconducting quantum interference device (SQUID) magnetometer after each step.

3.3. Paleointensity

A total of 246 specimens from 41 samples were processed for paleointensity experiments with a minimum of 5 specimens per sample. Before the intensity experiment, samples were broken into irregular chips and fresh specimens were selected. For the convenience of orienting during the experiment, the irregular chip specimens were fixed in cubic ceramic boxes (1.2 cm × 1.2 cm × 1.2 cm) with fire-resistant cotton matting. The ceramic cubes have comparable magnetic moments to the background of the magnetometer used for the measurements and do not contaminate the magnetic signal of the specimens. The procedure for the paleointensity experiment followed the "IZZI" protocol suggested by *Tauxe and Staudigel* [2004]. Of all the specimens, 166 specimens were heated in a French paleointensity furnace in an argon atmosphere. Specimens cool naturally after the heating, which takes ~12 h. The rest of 80 specimens were processed in the MMTDSC oven mentioned above. This oven is fixed with a fan and has a much faster cooling time of about 20 min. The residual field of both ovens is less than 10 nT for the "zero field" cooling steps. Heating steps were carried out from 100°C to 580°C with temperature intervals varying from 20°C to 100°C. The laboratory field of 30 μT is applied along $-z$ axis of the specimens with a precision of 0.1 μT for the "in field" cooling steps. The remanence was measured with the 2G 760 SQUID magnetometer after each step. The whole procedure of the experiment was conducted in a shielded room with residual field less than 300 nT.

The bias in paleointensity caused by anisotropy of thermal remanent magnetism (ATRM) in archaeological study is nontrivial [*Rogers et al.*, 1979; *Aitken et al.*, 1981, 1988]. ATRM correction was conducted on each successful specimen in the intensity experiment following the method of *Veitch et al.* [1984]. A total TRM was used for the calculation of the anisotropy tensors. An alteration check step was added to monitor any thermal alteration during the experiment.

The effect of cooling rate is also considered in this study. Only specimens heated in the MMTDSC oven underwent cooling rate corrections. It is not necessary for those processed in the French furnace because the natural cooling system mimics the original cooling of the pottery when first fired. The cooling rate correction experiment follows the procedure suggested by *Genevey and Gallet* [2002]. Specific experimental steps could be found in *Cai et al.* [2014].

4. Results

4.1. Dating Results

The radiocarbon dating results are shown in Table 2 and Figure 2. The calibration software of OxCal v4.2.3 [*Ramsey et al.*, 2013] and calibration curve of IntCal13 [*Reimer et al.*, 2013] were employed. The age spectrum

Table 2. The Radiocarbon Dating Results[a]

Sample ID	Laboratory No.	Material	Age_{meas}/B.P.	$^{13}C/^{12}C$/‰	Age_{conv}/B.P.	Age_{cal}/B.P.
2012SJLY1	Beta-348495	charred material	4220 ± 30	−22.5	4260 ± 30	4870–4816
2012SJLY3	Beta-348496	charred material	4100 ± 30	−23.9	4120 ± 30	4726–4528
2012SJLY4	Beta-348497	charred material	4340 ± 30	−20.5	4410 ± 30	5055–4866
2012SJLY5	Beta-348498	bone collagen	4320 ± 30	−20.5	4390 ± 30	5041–4867
2012SJLY8	Beta-348499	charred material	4130 ± 30	−23.8	4150 ± 30	4773–4577

[a] Age_{meas} is the measured radiocarbon age. Age_{conv} is the conventional radiocarbon age. Age_{cal} is the final age calibrated with the curve of IntCal13. The present in "B.P." means 1950 C.E.

with largest probability for each sample was used in this study. The radiocarbon ages of materials collected from different kilns are adopted to approximate the age of the kilns. Therefore, the final ages of Y1, Y3, Y4, Y5, and Y8 are 4870–4816 B.P., 4726–4528 B.P., 5055–4866 B.P., 5041–4867 B.P., and 4773–4577 B.P., respectively.

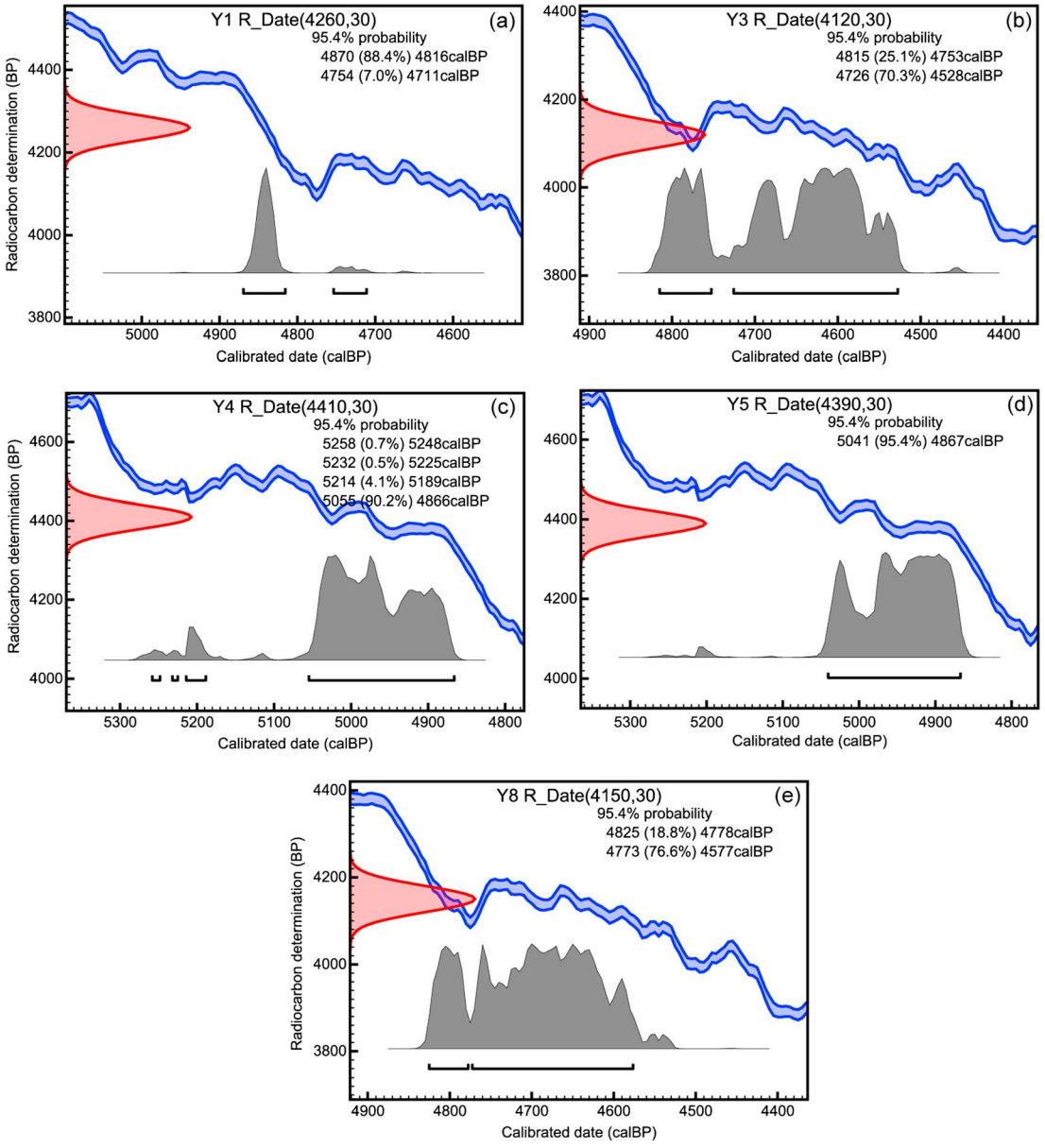

Figure 2. Calibration results of radiocarbon dating. The calibrated ages and their probability are shown in the plots. The "present" in B.P. means 1950 C.E. The version of calibration software is OxCal v4.2.3 [*Ramsey et al.*, 2013], and the calibration curve is IntCal13 [*Reimer et al.*, 2013].

Table 3. The OSL Dating Results of the Two Potteries[a]

Sample ID	U (ppm)	Th (ppm)	K (%)	Grain Size (μm)	Dose Rate (Gy/ka)	De (Gy)	Age (ka)
LJZ1c	1.76	12.30	2.23	90–125	3.60 ± 0.18	17.624 ± 0.228	4.895 ± 0.253
LJZ4a	2.40	16.50	2.52	4–11	4.47 ± 0.22	20.659 ± 0.567	4.622 ± 0.260

[a]U (ppm), Th (ppm), and K (%) are the concentrations of uranium, thorium, and potassium involved in the samples. The grain size represents the size of quartz fraction used for age determination. De is the equivalent dose.

All statistics and dating results of the OSL dating are listed in Table 3. The final ages of LJZ1c and LJZ4a are 4.895 ± 0.253 ka and 4.622 ± 0.260 ka, respectively, which are consistent with the radiocarbon dating results, demonstrating the accuracy of both ages.

Besides the dating methods mentioned above, the stratigraphic information of the cultural layers and archaeointensity results are considered to supply further constraints on the sample ages. It is believed by

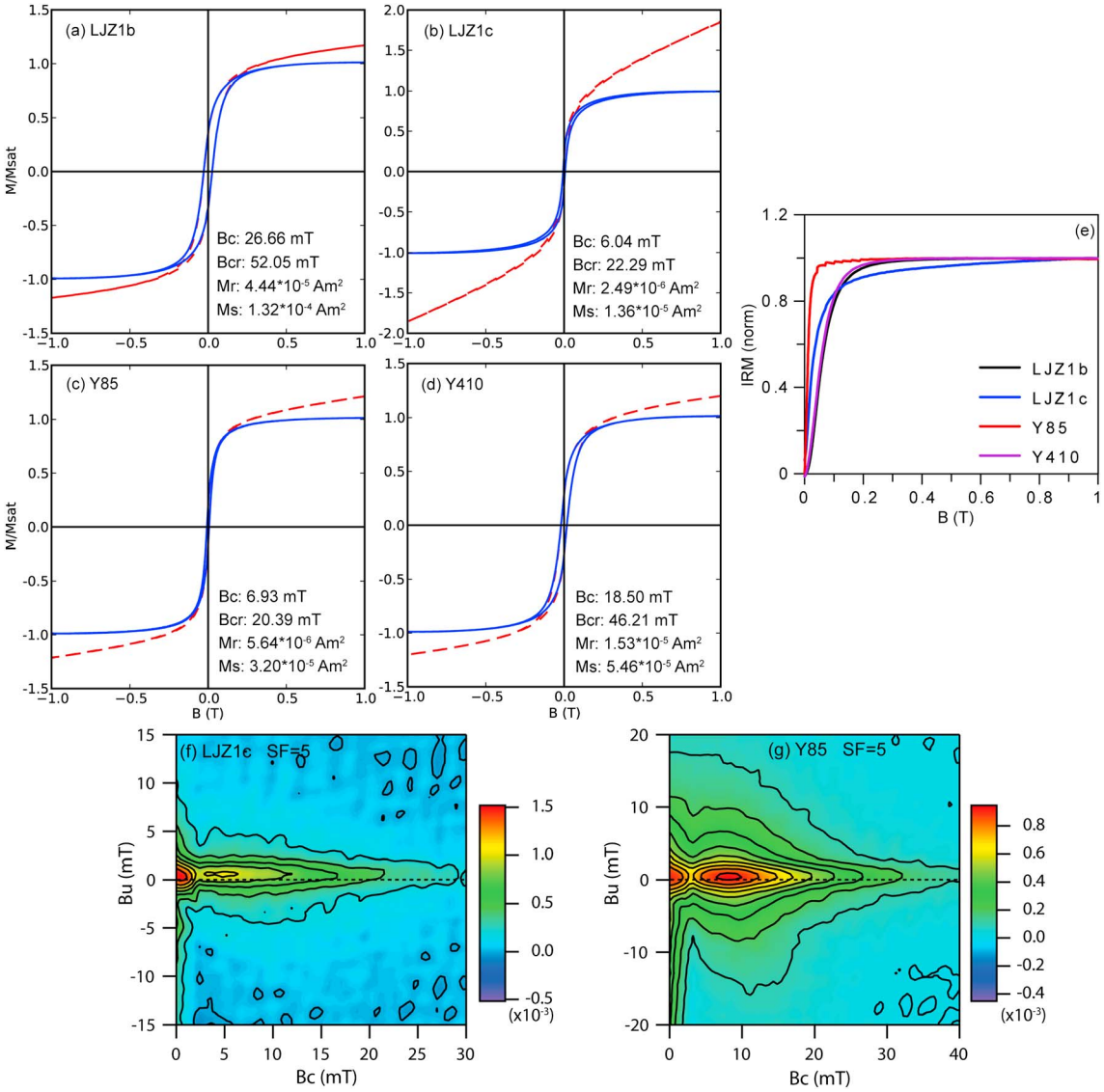

Figure 3. (a–d) Hysteresis loops of representative samples. The red (blue) loop is before (after) paramagnetic correction. The hysteretic parameters, B_c: coercivity, B_{cr}: remanent coercivity, M_r: remanent magnetization, and M_s: saturated magnetization, are listed on the plots. Data are analyzed with the software of Pmagpy-2.184 by Lisa Tauxe. (e) IRM acquisition curves of representative samples. (f and g) FORC plots after *Roberts et al.* [2000]. Data are analyzed with the software of FORCinel_1.17.

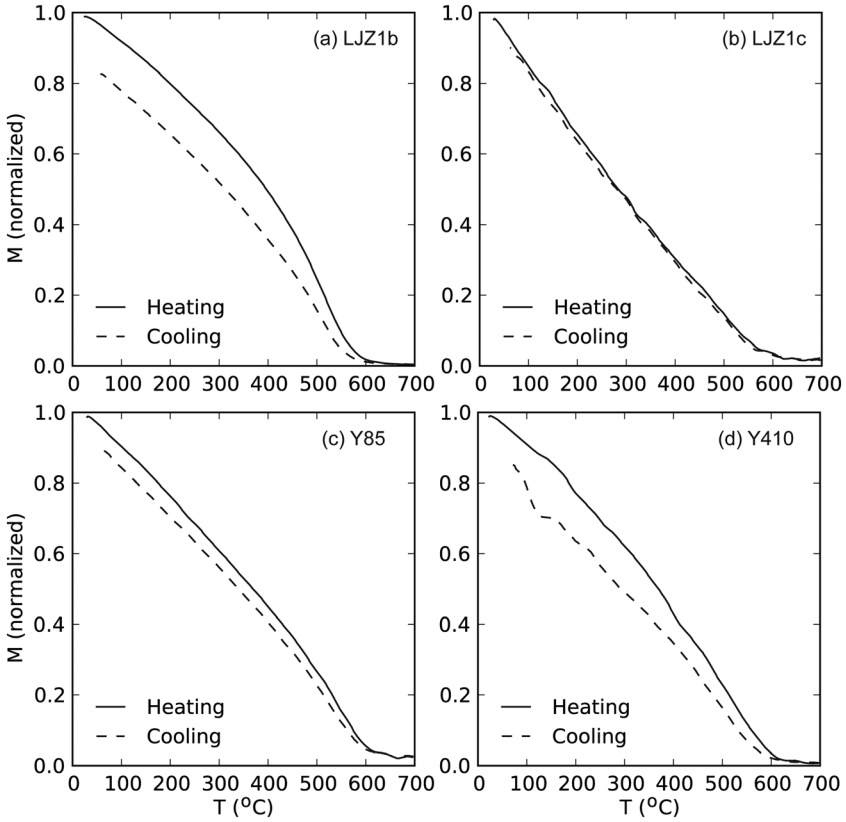

Figure 4. Representative variations of normalized magnetization versus temperature. Samples are processed in air in an applied field of ~1 T with heating/cooling rates of 30°C/min. The solid (dashed) line represents the heating (cooling) procedure.

archaeologists that relics associated with the same cultural layers generally have similar ages. In addition, samples belonging to the same period should yield identical archaeointensity values within the error. Therefore, more precise age controls could be reached if we combine the stratigraphic and archaeointensity information. For example, Y1 and Y2 are both in Layer I and thus can rely on the radiocarbon age of Y1. LJZ4a and LJZ4e are both in Layer III and record approximate intensity values, which could share the OSL age of LJZ4a. The final age after combining all the information of radiocarbon analysis, OSL dating, stratigraphic relationship, and archaeointensity results are listed in Tables 1 and 5.

4.2. Rock Magnetic Results

The hysteresis loops of representative specimens show slightly wasp-waisted shapes (Figures 3a–3d), indicating a mixing of different grain sizes or minerals [*Tauxe et al.*, 1996]. The hysteresis parameters inferred from the bulk measurements are shown on the figures, but these are difficult to interpret in the case of mixtures of different populations. The bulk coercivity (B_c) ranges from ~10 mT to ~30 mT, which demonstrates that soft magnetic minerals are the dominant magnetic carriers. This inference is supported by the IRM acquisition curves (Figure 3e), which generally saturate before 200 mT (except for LJZ1c which does not saturate by 1 T). Further evidence is from the shape of FORCs (Figures 3f and 3g), which indicate a single domain fraction mixed with limited multidomain (MD) or superparamagnetic grains.

The *M-T* curves show good reversibility (Figure 4), indicating slight or no alteration during heating. Curie temperatures (T_c) calculated by the second derivative method described by *Tauxe et al.* [2010] are ~580°C or slightly lower, demonstrating magnetite or Ti-poor titanomagnetite as the main magnetic minerals. Representative three-axis IRM demagnetization curves (Figure 5) show a low-coercivity component ($<$0.15 T) being dominant, and all three components are totally demagnetized before 600°C (except for LJZ1c), which

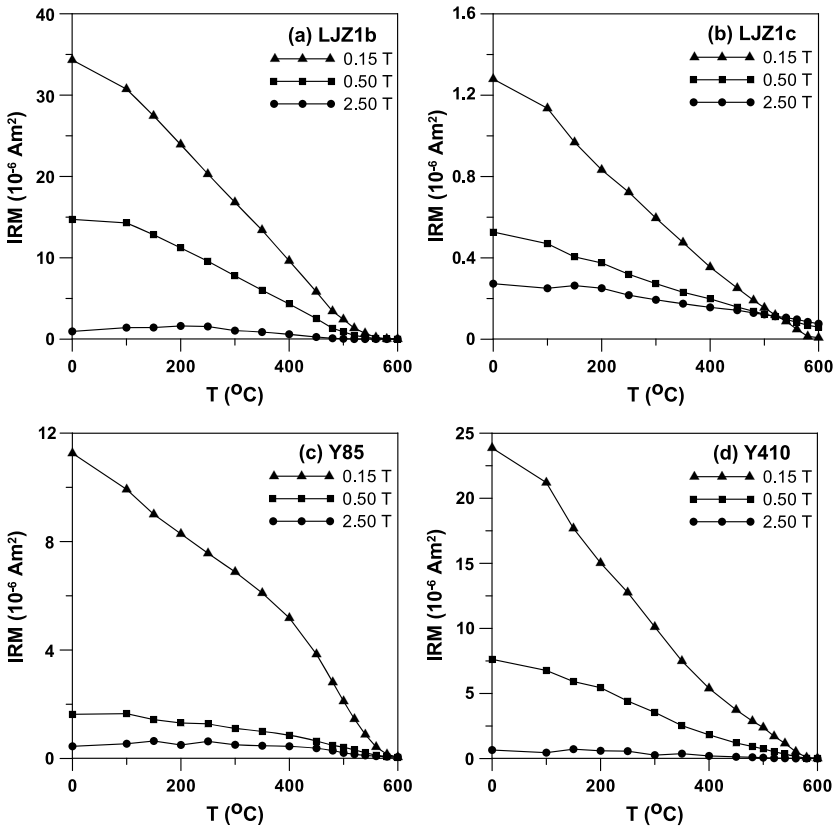

Figure 5. Representative three-axis IRM demagnetization results. The triangles/ squares/solid circles represent the demagnetization steps on the direction of minimum (0.15 T)/middle (0.5 T)/maximum (2.5 T) fields.

agrees with the conclusion of magnetite or titanomagnetite being the dominant magnetic carriers obtained from the *M-T* results. The results for LJZ1c are consistent with a hematite remanence, however.

4.3. Paleointensity Results

A great number of selection criteria have been put forward to estimate the reliability of paleointensity results [*Paterson et al.*, 2014]. We use the most common and effective selection statistics in this study (Table 4), as well as some new ones proposed by *Shaar and Tauxe* [2013]. The detailed description of each statistic can be found in *Paterson et al.* [2014] and *Cai et al.* [2014] and references therein. Based on the selection criteria, 141 out of 246 specimens from 29 samples are considered to yield robust paleointensity estimates, with a success rate of ~57%. The results of accepted samples are listed in Table 5; those on specimen level are listed in Table S1 in the supporting information. Representative accepted specimens are shown in Figures 6a and 6b, which typically behave linearly on the Arai plots and have a single-directional component trending to the origin except a small secondary component removed by 100-150°C in the orthogonal projection plots (Figures 6a2 and 6b2). Specimens are generally rejected either by nonlinear behavior on the Arai plots (Figure 6c) or nonideal behavior on the orthogonal projection plots (Figure 6d2). The former is usually caused by alteration during the paleointensity experiments, MD effects [*Dunlop and Xu*, 1994; *Xu*

Table 4. Data Selection Criteria Adopted for Paleointensity Results in This Study[a]

β	DANG	MAD	DRATS	f	f_{vds}	FRAC	SCAT	alter_atrm	alter_cool	N_{min}	σ/% or σ
≤0.1	≤8	≤10	≤10	≥0.6	≥0.5	≥0.6	Pass	≤10%	≤5%	≥3	≤10% or 5 μT

[a]FRAC and SCAT are two statistics defined by *Shaar and Tauxe* [2013]. The description of other statistics can be found in *Cai et al.* [2014].

Table 5. The List of Accepted Results on Sample Level[a]

Sample	Age/B.C.E.	σ_{Age}/a	B_{lab}	B_{acc}	σ_B	σ_B/%	VADM	σ_{VADM}	n_a
			μT				$\times10^{22}$ Am^2		
LJZ1a	3100	250	30	14.82*	0.65	4.39	2.83	0.12	5
LJZ1c	2895	253	30	33.06*	3.96	11.98	6.31	0.76	5
LJZ1d	3004	87	30	27.58*	1.38	5.00	5.26	0.26	6
LJZ2b	2893	27	30	37.89*	1.12	2.96	7.23	0.21	7
LJZ2c	3004	87	30	26.22*	1.25	4.77	5.00	0.24	5
LJZ2d	3004	87	30	28.06*	0.66	2.35	5.36	0.13	5
LJZ3c	3011	95	30	34.62*	1.59	4.59	6.61	0.30	6
LJZ3d	2725	98	30	41.00*	2.93	7.15	7.82	0.56	3
LJZ3e	3011	95	30	32.27*	0.32	0.99	6.16	0.06	4
LJZ4a	2622	260	30	25.05*	2.67	10.66	4.78	0.51	6
LJZ4e	2622	260	30	21.56*	3.84	17.81	4.11	0.73	5
LJZ4f	2725	98	30	36.24*	0.80	2.21	6.92	0.15	5
Y22a	2893	27	30	34.13*	2.19	6.42	6.51	0.42	6
Y23a	2893	27	30	38.45*	0.50	1.30	7.34	0.10	6
Y23b	2893	27	30	35.70*	2.58	7.23	6.81	0.49	6
Y23c	2893	27	30	38.50*	0.77	2.00	7.35	0.15	6
Y32i	2677	99	30	28.07	1.49	5.31	5.36	0.28	5
Y35a	2677	99	30	32.25*	3.06	9.49	6.15	0.58	6
Y42i	3011	95	30	23.77	4.77	20.07	4.54	0.91	5
Y48a	3011	95	30	26.93*	2.38	8.84	5.14	0.45	6
Y49a	3011	95	30	34.47*	1.40	4.06	6.58	0.27	3
Y51i	3004	87	30	27.49	3.33	12.11	5.25	0.64	3
Y52i	3004	87	30	23.78	3.12	13.12	4.54	0.60	3
Y55i	3004	87	30	32.05	1.03	3.21	6.12	0.20	3
Y61i	3011	95	30	27.95	4.41	15.78	5.33	0.84	6
Y75a	3011	95	30	19.88*	0.30	1.51	3.79	0.06	4
Y81i	2725	98	30	35.22	1.04	2.95	6.72	0.20	4
Y84a	2725	98	30	35.97*	2.58	7.17	6.86	0.49	3
Y85a	2725	98	30	40.33*	3.11	7.71	7.70	0.59	4

[a] B_{lab}: applied field in the lab, B_{acc}: average paleointensity of a sample after anisotropy and cooling rate correction (those without cooling rate correction are marked with an "asterisk"), σ_B: standard deviation of B_{acc}, σ_{VADM}: standard deviation of VADM, n_a: number of specimens accepted.

and Dunlop, 1994], or multiple components, while the latter is often induced by overprint of secondary components (perhaps acquired by reheating during cooking or fires).

The anisotropy and cooling rate correction results are shown in Figure 7. Alteration during the anisotropy correction experiment is usually less than 10% (Figure 7a), and those with more than 10% are excluded. The ratio of maximum and minimum eigenvalues of the ATRM tensors (τ_1/τ_3) varies between 1.03 and 1.83. The extent of anisotropy correction is generally less than 10% with few exceptions of 30%-40% (Figure 7b). After ATRM correction, 76% (22/29) of the samples yield more concentrated average intensities, demonstrating the validity of the anisotropy correction. A cooling rate correction is only applied on the specimens processed with the MMTDSC oven. The alteration during cooling rate experiment is quite limited (<2%; Figure 7c), and the amount of cooling rate correction ranges from 3% to 7% (Figure 7d).

5. Discussion

The important geophysical location of China near the CAA makes the variation of the geomagnetic field in this area of particular interest. However, reliable paleointensity data with modern experimental procedures and stringent selection criteria are scarce or nonexistent. High-fidelity archaeointensity data with precise age constraints around 3000 B.C.E. obtained from Sichuan Liujiazhai site in southwestern China can fill spatial and temporal gaps in the published data sets.

We pull together various dating techniques to control the sample ages as precisely as possible. The radiocarbon ages from the kilns and the OSL ages from the two pottery samples are generally consistent,

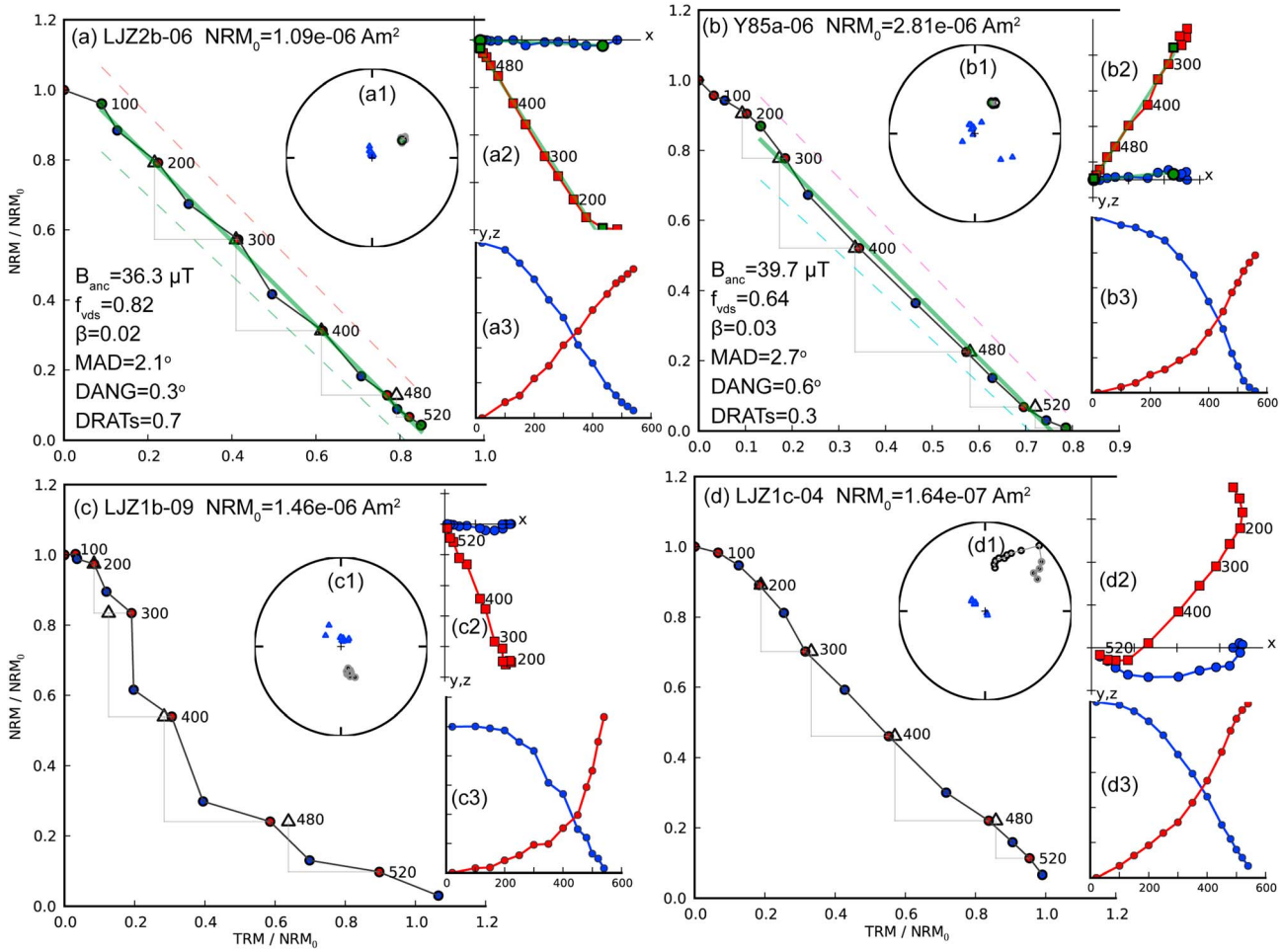

Figure 6. (a1–d1) Arai plots and the relative equal area projections, (a2–d2) orthogonal projections, and (a3–d3) natural remanent magnetism lost-TRM (thermal remanent magnetism) gained curves of representative (a and b) accepted and (c and d) rejected specimens. The numbers on the Arai plot and orthogonal projections are temperature steps in centigrade (°C). The description of the statistics in the figure can be found in *Cai et al.* [2014] and *Shaar and Tauxe* [2013]. Detailed introduction of each figure can be found in *Shaar and Tauxe* [2013]. The plots are made with the software of Thellier_GUI [*Shaar and Tauxe*, 2013].

demonstrating the reliability of the ages. The stratigraphic information and archaeological and archaeomagnetic estimations are combined to further control the sample ages. Well-constrained ages in this study supply more details of the geomagnetic field variations.

Rock magnetic results of the studied samples indicate thermally stable, fine-grained magnetite, or titanomagnetite as the dominant magnetic carriers in most instances, which assure their suitability for paleointensity determinations. A high success rate of ~57% (141/246) is obtained during the intensity experiment. The new results in this study as well as the published paleointensity data from the Magnetics Information Consortium (MagIC) database (http://earthref.org/MAGIC) in eastern Asia are shown in Figure 8. The following selection criteria are applied: the data must be obtained through a double-heating protocol and be based on averages of at least three specimens and have a standard deviation of mean intensity less than 10% or 5 μT.

The VADMs (virtual axial dipole moments) of the new data vary from approximately (2.8 to 7.8) $\times 10^{22}$ Am^2 with an average of 5.9×10^{22} Am^2, which is lower than the present field intensity (9.8×10^{22} Am^2) in the sampling site. The high-fidelity intensity data together with well-constrained ages have shown that the variations of geomagnetic intensity are serially correlated and follow a reverse "U" shape between ~3100 B.C.E. and ~2600 B.C.E. (see inset in Figure 8). The rate during the initial increase from about ~3100 B.C.E. to ~2900 B.C.E. is about 10 μT/century comparable to the rate during the subsequent decay from ~2750 B.C.E. to ~2600 B.C.E., while the average variation rate during the 500 years is ~5 μT/century. These

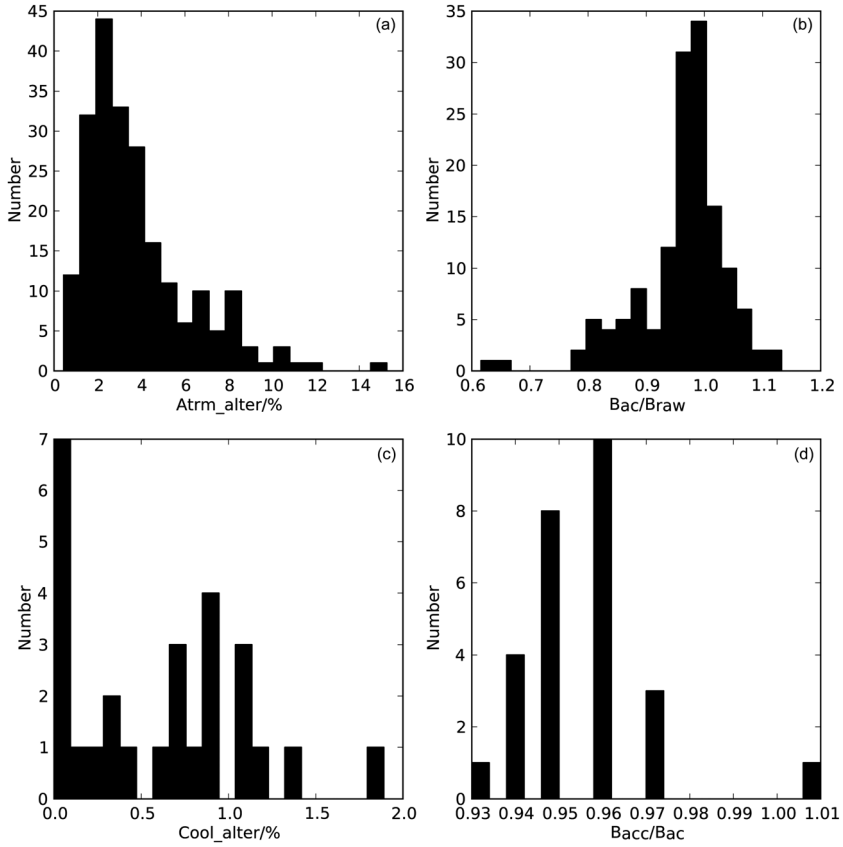

Figure 7. Histograms of (a) alteration percent during the TRM anisotropy correction experiment, (b) extent of TRM anisotropy correction described by the ratio of intensity value after anisotropy correction (B_{ac}) to the raw intensity (B_{raw}), (c) alteration percent during cooling rate correction experiment, and (d) cooling rate correction factors expressed as the ratio of intensity after both anisotropy and cooling rate correction (B_{acc}) to B_{ac}.

estimates are under the upper bounds of ~0.62 μT/yr, calculated through numerical models by *Livermore et al.* [2014]. When cast as %/decade, these rates (~4%/decade) are comparable to those observed by *Shaar et al.* [2015].

We record two periods of low intensity (decreases in paleointensity (DIPs)) in this study with VADMs of less than or around 4×10^{22} Am^2. The first is as low as ~2.8×10^{22} Am^2 at ~3100 B.C.E. The more recent DIP, with an age of ~2650 B.C.E. and a value of ~4×10^{22} Am^2, just predates the DIP of ~2.3×10^{22} Am^2 reported by *Cai et al.* [2014] at about ~2250 B.C.E. It is possible that the two extreme lows at ~3100 B.C.E. and ~2250 B.C.E. are the same feature, and the age difference is just caused by loose age control (both are based on archaeological estimation). That said, a difference of nearly 1000 years is difficult to attribute to archaeological dating errors. It is perhaps more likely that the two lows are separate features of the geomagnetic field at different time periods. In this interpretation, the downward trending data between ~2750 B.C.E. and ~2600 B.C.E. recovered in this study are the onset of the DIP at ~2250 B.C.E. documented by *Cai et al.* [2014]. More reliable data with better age constraints are needed to resolve this issue. In any case, the low intensities reported here could be taken as a further evidence of the existence of broad "DIP" during the period of ~3000-2000 B.C.E. The new results from this study are generally consistent with the published data with similar age but deviate significantly from the CALS10k.1b model at certain time period (thick grey line in Figure 8). Our new results should therefore be incorporated into future secular variation models.

The globally published paleointensity data since 10 ka are mainly concentrated in the past 3 kyr (see Figure S1 in the supporting information in *Mitra et al.* [2013]), and data from more ancient periods are scarce. The new results from Liujiazhai site in this paper are significant for constraining the variation of geomagnetic field between ~3100 and 2600 B.C.E. Since most of the published data in China are from the eastern part, the new

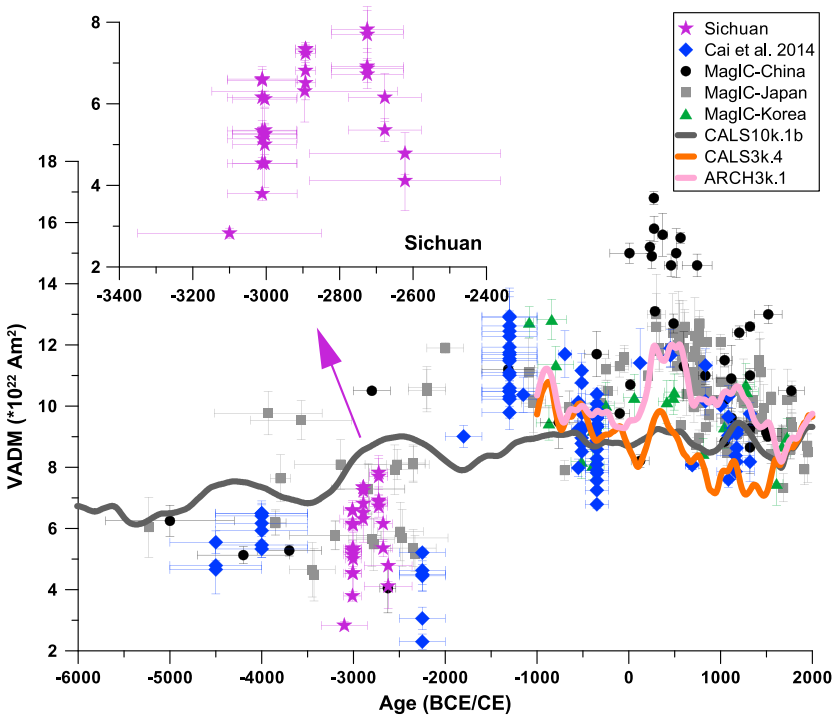

Figure 8. Variation of VADMs in this study and their comparison with published data in eastern Asia and predictions of global models. The black solid circles/grey squares/green triangles up are the accepted published data in China/Japan/Korea [*Hong et al.*, 2013] from MagIC database. For data selection criteria, please see the text. The magenta stars/blue diamonds represent the new data of this study/published data in *Cai et al.* [2014]. The grey/orange/pink line is the prediction from global model of CALS10k.1b [*Korte et al.*, 2011]/CALS3k.4 [*Korte and Constable*, 2011]/ARCH3k.1 [*Korte et al.*, 2009] at the center of China (35°N, 105°E).

results from Sichuan Liujiazhai site in southwestern China could improve the spatial distribution of data and have potential applications for regional comparisons in the future. The new data set is also useful for improving the regional geomagnetic model of eastern Asia, which has great implications for future archaeomagnetic dating in this area.

6. Conclusions

In this paper, we carried out a detailed archaeomagnetic study on late Neolithic remains at the Liujiazhai archaeological site in Sichuan province, southwestern China. The main conclusions drawn from this study are as follows:

1. The radiocarbon ages from the kilns range from ~3000 to 2600 B.C.E., while the OSL ages from the two potteries are ~2900 BC (LJZ1c) and ~2600 B.C.E. (LJZ4a), respectively. The consistency between two dating techniques assures the reliability of the ages. Further information from stratigraphic relationship and archaeological and archaeomagnetic estimation provides more constraints on the sample ages.
2. Detailed rock magnetic studies indicate thermally stable, fine-grained magnetite or titanomagnetite as the dominant magnetic carriers, which assure their suitability to paleointensity determinations.
3. The VADMs of the new data vary from approximately 2.8 to 7.8×10^{22} Am^2 with an average of 5.9×10^{22} Am^2, indicating that the geomagnetic intensity around 3000 B.C.E. is overall lower than the present field intensity (9.8×10^{22} Am^2) of this area.
4. We observe a period of rapid field growth followed by rapid field decay. Both exhibit changes of some 10 μT/century (translating to some 4%/decade), under the upper-bound values predicted by *Livermore et al.* [2014], and consistent with those observed by *Shaar et al.* [2015].
5. A low-intensity value (~2.3×10^{22} Am^2) with the DIP was reported by *Cai et al.* [2014] at ~2250 B.C.E. We observe comparable values of ~2.8×10^{22} Am^2 at ~3100 B.C.E. This DIP may be the same as that reported in the early study; alternatively, there is a second DIP with comparable field values preceding the DIP of

Cai et al. [2014] by ~1000 years. In any case, the new data constitute further evidence of the existence of a broad low in the geomagnetic intensity in China during the period of ~3000-2000 B.C.E.

6. The new results from this study supply important data for future versions of the global paleosecular variation models and are significant for constraining the variation of geomagnetic field between ~3100 and 2600 B.C.E. The new data set are also useful for improving the regional geomagnetic model of eastern Asia, which has great implications for future archaeomagnetic dating in this area.

Acknowledgments

We thank Li Qin and Guangbiao Wei for their assistance in the sample collection. We thank the great help from Zhijun Gong and Jimin Sun during the OSL dating. This work was funded by the NSFC grant 41274073 and the 973 program grant 2012CB821900. C.D. acknowledges further support from the CAS Bairen Program. L.T. acknowledges support from grant EAR 1141840. Shuhui Cai was funded by the China Postdoctoral Science Foundation. All the published paleointensity data used in this paper can be found in the MagIC database (http://earthref.org/MAGIC). All the new data and interpretations in this study have been uploaded into the MagIC database as private (http://earthref.org/MAGIC/search/#10067), which are available with the group name (Sichuan) and group password (ljz123).

References

Aguilar Reyes, B., A. Goguitchaichvili, J. Morales, V. H. Garduño, M. Pineda, C. Carvallo, T. G. Moran, I. Israde, and M. C. Rathert (2013), An integrated archeomagnetic and C14 study on pre-Columbian potsherds and associated charcoals intercalated between Holocene lacustrine sediments in Western Mexico: Geomagnetic implications, *J. Geophys. Res. Solid Earth*, *118*, 2753–2763, doi:10.1002/jgrb.50196.

Aitken, M. J. (1998), *An Introduction to Optical Dating*, 279 pp., Oxford Univ. Press, Oxford, U. K.

Aitken, M. J., P. Alcock, G. D. Bussell, and C. Shaw (1981), Archaeomagnetic determination of the past geomagnetic intensity using ancient ceramics: Allowance for anisotropy, *Archaeometry*, *23*, 53–64.

Aitken, M. J., A. L. Allsop, G. D. Bussell, and M. B. Winter (1988), Determination of the intensity of the Earth's magnetic field during archeological times: Reliability of the Thellier technique, *Rev. Geophys.*, *26*, 3–12, doi:10.1029/RG026i001p00003.

Amit, H., M. Korte, J. Aubert, C. Constable, and G. Hulot (2011), The time-dependence of intense archeomagnetic flux patches, *J. Geophys. Res.*, *116*, B12106, doi:10.1029/2011JB008538.

Bard, E., and G. Delaygue (2008), Comment on "Are there connections between the Earth's magnetic field and climate?", *Earth Planet. Sci. Lett.*, *265*(1–2), 302–307.

Ben-Yosef, E., L. Tauxe, H. Ron, A. Agnon, U. Avner, M. Najjar, and T. E. Levy (2008), A new approach for geomagnetic archaeointensity research: Insights on ancient metallurgy in the Southern Levant, *J. Archaeol. Sci.*, *35*(11), 2863–2879, doi:10.1016/j.jas.2008.05.016.

Ben-Yosef, E., L. Tauxe, and T. E. Levy (2010), Archaeomagnetic dating of copper smelting site F2 in the Timna Valley (Israel) and its implications for the modelling of ancient technological developments, *Archaeometry*, *52*, 1110–1121.

Biggin, A. J., M. J. de Wit, C. G. Langereis, T. E. Zegers, S. Voûte, M. J. Dekkers, and K. Drost (2011), Palaeomagnetism of Archaean rocks of the Onverwacht Group, Barberton Greenstone Belt (southern Africa): Evidence for a stable and potentially reversing geomagnetic field at ca. 3.5 Ga, *Earth Planet. Sci. Lett.*, *302*(3–4), 314–328.

Biggin, A. J., B. Steinberger, J. Aubert, N. Suttie, R. Holme, T. Torsvik, D. van der Meer, and D. van Hinsbergen (2012), Possible links between long-term geomagnetic variations and whole-mantle convection processes, *Nat. Geosci.*, *5*(8), 526–533.

Bloxham, J. (2000), Sensitivity of the geomagnetic axial dipole to thermal core-mantle interactions, *Nature*, *405*(6782), 63–65.

Bloxham, J., S. Zatman, and M. Dumberry (2002), The origin of geomagnetic jerks, *Nature*, *420*(6911), 65–68.

Cai, S., L. Tauxe, C. Deng, Y. Pan, G. Jin, J. Zheng, F. Xie, H. Qin, and R. Zhu (2014), Geomagnetic intensity variations for the past 8 kyr: New archaeointensity results from Eastern China, *Earth Planet. Sci. Lett.*, *392*, 217–229.

Courtillot, V., Y. Gallet, J. L. Mouël, F. Fluteau, and A. Genevey (2007), Are there connections between the Earth's magnetic field and climate?, *Earth Planet. Sci. Lett.*, *253*(3–4), 328–339.

Dumberry, M., and C. C. Finlay (2007), Eastward and westward drift of the Earth's magnetic field for the last three millennia, *Earth Planet. Sci. Lett.*, *254*(1–2), 146–157.

Dunlop, D. J., and S. Xu (1994), Theory of partial thermoremanent magnetization in multidomain grains: I. Repeated identical barriers to wall motion (single microcoercivity), *J. Geophys. Res.*, *99*, 9005–9023, doi:10.1029/93JB02566.

Gallet, Y., A. Genevey, and F. Fluteau (2005), Does Earth's magnetic field secular variation control centennial climate change?, *Earth Planet. Sci. Lett.*, *236*, 339–347.

Gallet, Y., M. D'Andrea, A. Genevey, F. Pinnock, M. Le Goff, and P. Matthiae (2014), Archaeomagnetism at Ebla (Tell Mardikh, Syria). New data on geomagnetic field intensity variations in the Near East during the Bronze Age, *J. Archaeol. Sci.*, *42*, 295–304.

Genevey, A., and Y. Gallet (2002), Intensity of the geomagnetic field in western Europe over the past 2000 years: New data from French ancient pottery, *J. Geophys. Res.*, *107*(B11), 2285, doi:10.1029/2001JB000701.

Hong, H., Y. Yu, C. H. Lee, R. H. Kim, J. Park, S.-J. Doh, W. Kim, and H. Sung (2013), Globally strong geomagnetic field intensity circa 3000 years ago, *Earth Planet. Sci. Lett.*, *383*, 142–152.

Hori, K., J. Wicht, and W. Dietrich (2014), Ancient dynamos of terrestrial planets more sensitive to core-mantle boundary heat flows, *Planet. Space Sci.*, *98*, 30–40.

Kent, D. V. (1982), Apparent correlation of palaeomagnetic intensity and climatic records in deep-sea sediments, *Nature*, *299*, 538–539.

Korte, M., and C. Constable (2011), Improving geomagnetic field reconstructions for 0–3 ka, *Phys. Earth Planet. Inter.*, *188*(3–4), 247–259.

Korte, M., F. Donadini, and C. G. Constable (2009), Geomagnetic field for 0–3 ka: 2. A new series of time-varying global models, *Geochem. Geophys. Geosyst.*, *10*, Q06008, doi:10.1029/2008GC002297.

Korte, M., C. Constable, F. Donadini, and R. Holme (2011), Reconstructing the Holocene geomagnetic field, *Earth Planet. Sci. Lett.*, *312*(3–4), 497–505.

Livermore, P. W., A. Fournier, and Y. Gallet (2014), Core-flow constraints on extreme archeomagnetic intensity changes, *Earth Planet. Sci. Lett.*, *387*, 145–156.

Lowrie, W. (1990), Identification of ferromagnetic minerals in a rock by coercivity and unblocking temperature properties, *Geophys. Res. Lett.*, *17*, 159–162, doi:10.1029/GL017i002p00159.

Mandea, M., R. Holme, A. Pais, K. Pinheiro, A. Jackson, and G. Verbanac (2010), Geomagnetic jerks: Rapid core field variations and core dynamics, *Space Sci. Rev.*, *155*(1–4), 147–175.

Mitra, R., L. Tauxe, and S. K. McIntosh (2013), Two thousand years of archeointensity from West Africa, *Earth Planet. Sci. Lett.*, *364*, 123–133.

Olsen, N., and M. Mandea (2008), Rapidly changing flows in the Earth's core, *Nat. Geosci.*, *1*(6), 390–394.

Pan, Y., and R. Zhu (2011), A review of biogeophysics: The establishment of a new discipline and recent progress, *Chin. Sci. Bull.*, *56*(17), 1335–1344.

Paterson, G. A., L. Tauxe, A. J. Biggin, R. Shaar, and L. C. Jonestrask (2014), On improving the selection of Thellier-type paleointensity data, *Geochem. Geophys. Geosyst.*, *15*, 1180–1192, doi:10.1002/2013GC005135.

Pavón-Carrasco, F. J., M. L. Osete, J. M. Torta, and L. R. Gaya-Piqué (2009), A regional archeomagnetic model for Europe for the last 3000 years, SCHA.DIF.3K: Applications to archeomagnetic dating, *Geochem. Geophys. Geosyst.*, *10*, Q03013, doi:10.1029/2008GC002244.

Pavón-Carrasco, F. J., J. Rodríguez-González, M. L. Osete, and J. M. Torta (2011), A Matlab tool for archaeomagnetic dating, *J. Archaeol. Sci.*, *38*(2), 408–419.
Prescott, J. R., and J. T. Hutton (1994), Cosmic-ray contributions to dose-rates for luminescence and ESR dating—Large depths and long-term time variations, *Radiat. Meas.*, *23*(2–3), 497–500.
Ramsey, C. B., E. M. Scott, and J. van der Plicht (2013), Calibration for archaeological and environmental terrestrial samples in the time range 26–50 ka cal BP, *Radiocarbon*, *55*(4), 2021–2027.
Reimer, P. J., et al. (2013), Intcal13 and Marine13 radiocarbon age calibration curves 0–50,000 years cal BP, *Radiocarbon*, *55*(4), 1869–1887.
Roberts, A. P., C. R. Pike, and K. L. Verosub (2000), First-order reversal curve diagrams: A new tool for characterizing the magnetic properties of natural samples, *J. Geophys. Res.*, *105*, 28,461–28,475, doi:10.1029/2000JB900326.
Rogers, J., J. M. W. Fox, and M. J. Aitken (1979), Magnetic anisotropy in ancient pottery, *Nature*, *277*(5698), 644–646.
Shaar, R., and L. Tauxe (2013), Thellier GUI: An integrated tool for analyzing paleointensity data from Thellier-type experiments, *Geochem. Geophys. Geosyst.*, *14*, 677–692, doi:10.1002/ggge.20062.
Shaar, R., L. Tauxe, E. Ben-Yosef, V. Kassianidou, B. Lorentzen, J. M. Feinberg, and T. E. Levy (2015), Decadal-scale variations in geomagnetic field intensity from ancient Cypriot slag mounds, *Geochem. Geophys. Geosyst.*, *16*, 195–214, doi:10.1002/2014GC005455.
Tarduno, J. A., R. D. Cottrell, M. K. Watkeys, A. Hofmann, P. V. Doubrovine, E. E. Mamajek, D. Liu, D. G. Sibeck, L. P. Neukirch, and Y. Usui (2010), Geodynamo, solar wind, and magnetopause 3.4 to 3.45 billion years ago, *Science*, *327*(5970), 1238–1240.
Tauxe, L., and H. Staudigel (2004), Strength of the geomagnetic field in the Cretaceous Normal Superchron: New data from submarine basaltic glass of the Troodos Ophiolite, *Geochem. Geophys. Geosyst.*, *5*, Q02H06, doi:10.1029/2003GC000635.
Tauxe, L., T. A. T. Mullender, and T. Pick (1996), Potbellies, wasp-waists, and superparamagnetism in magnetic hysteresis, *J. Geophys. Res.*, *101*, 571–583, doi:10.1029/95JB03041.
Tauxe, L., S. K. Banerjee, R. F. Butler, and R. van der Voo (2010), *Essentials of Paleomagnetism*, pp. 69–72, Univ. of Calif. Press, Berkeley.
Usui, Y., J. A. Tarduno, M. Watkeys, A. Hofmann, and R. D. Cottrell (2009), Evidence for a 3.45-billion-year-old magnetic remanence: Hints of an ancient geodynamo from conglomerates of South Africa, *Geochem. Geophys. Geosyst.*, *10*, Q09Z07, doi:10.1029/2009GC002496.
Veitch, R. J., I. G. Hedley, and J. J. Wagner (1984), An investigation of the intensity of the geomagnetic field during Roman times using magnetically anisotropic bricks and tiles, *Arch. Sci. (Geneva)*, *37*(3), 359–373.
Willis, A. P., B. Sreenivasan, and D. Gubbins (2007), Thermal core-mantle interaction: Exploring regimes for "locked" dynamo action, *Phys. Earth Planet. Inter.*, *165*(1–2), 83–92.
Wiltschko, R., and W. Wiltschko (2012), Magnetoreception, *Adv. Exp. Med. Biol.*, *739*, 126–141.
Xu, S., and D. J. Dunlop (1994), Theory of partial thermoremanent magnetization in multidomain grains: 2. Effect of microcoercivity distribution and comparison with experiment, *J. Geophys. Res.*, *99*, 9025–9033, doi:10.1029/93JB02571.
Yu, Y. J. (2012), High-fidelity paleointensity determination from historic volcanoes in Japan, *J. Geophys. Res.*, *117*, B08101, doi:10.1029/2012JB009368.